Electronic Supplementary Material (ESI) for Chemical Communications.
This journal is © The Royal Society of Chemistry 2019

Supporting Information

Gfp chromophore integrated conjugated microporous polymers: topological and ESPT effects on emission properties

Ashish Singh, Debabrata Samanta, Mrinal Boro and Tapas Kumar Maji*

Molecular Material Laboratory, Chemistry and Physics of Material Unit, School of Advance Material (SAMat), Jawaharlal Nehru Centre for Advanced Scientific Research, Jakkur, Bangalore-560064, India

*Email: tmaji@jncasr.ac.in
Tel: 91-8022082826

Table of Contents

Physical Measurements 3

Materials 4

Single-Crystal X-ray Diffraction 4

Experimental Section 5

(1) Photophysical studies 5

(2) Synthesis 5

(2a) Synthesis of *gfp* chromophore analgues (*o*-HBDI-I3 and *o*-MBDI-I3) 5

Synthetic scheme for *gfp* chromophore analogues

(2b) Synthesis of ((E)-2,4-diiodo-6-((4-iodophenylimino)methyl)phenol) (A) 6

(2c) Synthesis of methyl-2-(1-ethoxyethylideneamino)acetate (B) 6

(2d) Synthesis of the *ortho*-hydroxy substituted *gfp* chromophore (*o*-HBDI- 6

I3)

(2e) Synthesis of the *ortho*-methoxy substituted *gfp* chromophore (*o*-MBDI-I3) 7

(2f) Synthesis and synthetic scheme for 1,3,5-triethynylbenzene (TEB) 7

(2g) Synthesis of the *gfp* chromophore analogue containing CMPs (*o*-HBDI-TEB-CMP and *o*-HBDI-TEB-CMP) 8

Intra-molecular excited state proton transfer in *o*-HBDI-I3 9

Lifetime calculations 9

Theoretical calculations 10

Crystal data and structure refinement for *o*-HBDI-I3 and *o*-MBDI 12

Bond lengths table for *o*-HBDI-I3 13

Bond lengths table for *o*-MBDI-I3 13

2D extended crystal structure through non-covalent interactions of *o*-HBDI-I3 14

2D extended crystal structure through non-covalent interactions of *o*-MBDI-I3 14

C=O....π interactions in the *o*-MBDI-I3 14

^{1}H-NMR and ^{13}C-NMR for monomer *o*-HBDI-I3 15

^{1}H-NMR and ^{13}C-NMR for monomer *o*-HBDI-I3 16

Solvent dependent emission of *o*-HBDI-I3 17

Solvent dependent emission of *o*-MBDI-I3 18

TGA Analysis 18

EDX analysis for *o*-HBDI-TEB-CMP and *o*-MBDI-TEB-CMP 19

Overlapped IR spectra of *o*-HBDI-I3 and *o*-HBDI-TEB-CMP 20

Overlapped IR spectra of *o*-MBDI-I3 and *o*-MBDI-TEB-CMP 20

Pore size distribution for (a) *o*-HBDI-TEB-CMP and (b) *o*-MBDI-TEB-CMP 21

UV – spectrum for polymers 22

Solvent dependent emission of *o*-HBDI-TEB-CMP 23

Solvent dependent emission of *o*-MBDI-TEB-CMP 23

Dispersion stability test for o-HBDI-TEB-CMP 24

Solvent adsorption for polymers 24

pH dependent emission spectra for *o*-HBDI-TEB-CMP 25

Ground state and excited state geometry optimization for enol and keto form of monomer *o*-HBDI-I3 26

Schematic diagram for theoretically obtained energies for keto and enol form of *o*-HBDI-I3 in ground and excited state. 26

HOMO – LUMO calculation for enol form of polymer *o*-HBDI-TEB-CMP 27

Ground state and excited state geometry optimization for enol and keto form for polymer *o*-HBDI-TEB-CMP 27

HOMO – LUMO calculation for enol form of polymer *o*-MBDI-TEB-CMP 28

Ground state and excited state geometry optimization for polymer *o*-MBDI-TEB-CMP 28

References 29

Physical Measurements:

Bruker FT-IR spectrometer was used to record infrared spectra. Samples were prepared as pellets using KBr for IR measurement. Mettler Toledo-TGA 850 instrument was used to measure the thermal stability in N_2 atmosphere within the temperature range 30 - 800 °C at heating rate of 5 °C/min. Elemental analyses were performed in Thermo Scientific Flash 2000 CHN analyser. Powder X-ray diffraction patterns for both CMPs were recorded in Bruker D8 discover instrument using Cu-K∝ radiation. Morphological studies have been carried out using Lica-S440I Field Emission Scanning Electron Microscope (FESEM) by placing samples on a silicon wafer under high vacuum with an accelerating voltage of 100 kV. Transmission Electron Microscopy (TEM) analysis has been performed using JEOL JEM-3010 with an accelerating voltage at 300 kV. Energy dispersive spectroscopy (EDS) analysis was performed with an EDAX genesis instrument attached to the FESEM column. Varian infinity plus 300WB spectrometer was used to record the solid state ^{13}C-NMR spectra at a MAS rate of 5 kHz and a CP contact time of 1.4 ns. Adsorption measurements (N_2 (77 K)

and CO_2 (195 K)) were carried out in a QUANTACHROME QUADRASORD-SI analyser. The polymers, *o*-HBDI-TEB-CMP and *o*-MBDI-TEB-CMP are degassed at 160 °C and 1×10^{-1} Pa vacuum for 8 and 12 hrs, respectively, before the measurement of sorption isotherm. Solvent adsorption measurements (methanol at 293 K and benzene at 295 K) were carried out in the vapour state using BELSORP-aqua-3 volumetric adsorption instrument. UV-Vis studies were performed using Perkin Elmer Model Lambda 900 spectrophotometer instrument. The photoluminescence properties were performed in Fluorolog 3.21 spectrofluorimeter (Horiba Jobin-Yvon) instrument. Absolute quantum yield was measured for monomers and polymers using Edinburgh Instruments Steady State PL Spectrometer. The quantum yield measurement was performed by making dispersion of polymers in methanol. The lifetime studies were carried out using IBH-Data station platform. For the lifetime measurement, a nano-LED source with 370 nm was used for the *o*-HBDI-I3 and *o*-HBDI-TEB-CMP whereas 340 nm light was used for the *o*-MBDI-I3 and *o*-MBDI-TEB-CMP. ICP analysis was performed using a PerkinElmer Optima 7000 DV instrument.

Materials:

All the chemicals for the synthesis of the *gfp* chromophore analogues were procured from Sigma-Aldrich chemical Co. Ltd and used as such. Ethynyltrimethylsilane, Potassium carbonate and 1,3,5-tribromobenzene were obtained from Spectrochem Pvt. Ltd and used as such. Cuprous iodide was purchased from Loba Chemie Pvt. Ltd. Tetrakis(triphenylphosphine) palladium used as a catalyst for the synthesis of CMPs was purchased from Sigma-Aldrich chemical Co. Ltd. All the photophysical studies were carried out using HPLC grade solvents. For column chromatography, solvents were purchased from Finar Ltd, India and used as such. Deuterated chloroform ($CDCl_3$) was purchased from Sigma-Aldrich chemical Co. Ltd and used for ^{1}H and ^{13}C-NMR as such.

Single Crystal X-ray Diffraction:

Suitable single crystal of *o*-HBDI-I3 and *o*-MBDI-I3 was mounted on a thin glass fiber using commercially available glue. X-ray single-crystal data were collected on a Bruker Discovry D8 diffractometer equipped with a 2.4 kW sealed tube X-ray source with graphite monochromated Mo-Kα radiation (λ = 0.71073 Å) operating at 50 kV and 30 mA. The program SAINT[1] was used for the integration of diffraction profiles, and absorption correction was made with the SADABS[2] program. All the structures were solved by SHELXT[1] and refined by the fullmatrix least-squares method using SHELXL-2017.[3] All the

hydrogen atoms were fixed by HFIX and placed in ideal positions. The potential solvent accessible area or void space was calculated using the PLATON[4] multipurpose crystallographic software. All crystallographic and structure refinement data are summarized in Table S1. All calculations were carried out using SHELXL-2017[3] and WinGX system, Ver 1.80.05.[5]

Experimental Section:

1. **Photophysical studies:** Photophysical studies for monomers (*o*-HBDI-I3 and *o*-MBDI-I3) were carried out in solution state at room temperature. All the solutions were made up of 10^{-5} (M) concentration. The photophysics of CMPs were studied by making dispersion in different solvents. Both the CMPs were taken in different solvents and ground for 4-5 minutes in order to get good dispersion and subsequently photophysical experiments were performed.
2. **Synthesis:** Synthesis of *gfp* chromophore analogues, 1,3,5-triethynylbenzene and polymers is discussed separately as follows.

2a. Synthesis of *gfp* chromophore analgues (*o*-HBDI-I3 and *o*-MBDI-I3): For the synthesis of new analogues of the *gfp* chromophore (*o*-HBDI-I3 and *o*-MBDI-I3), we have adopted similar procedure as reported by Tolbert and co-workers.[6] The scheme of synthetic procedure is given in scheme S1. The chromophore (Z)-4-(2-hydroxy-3,5-

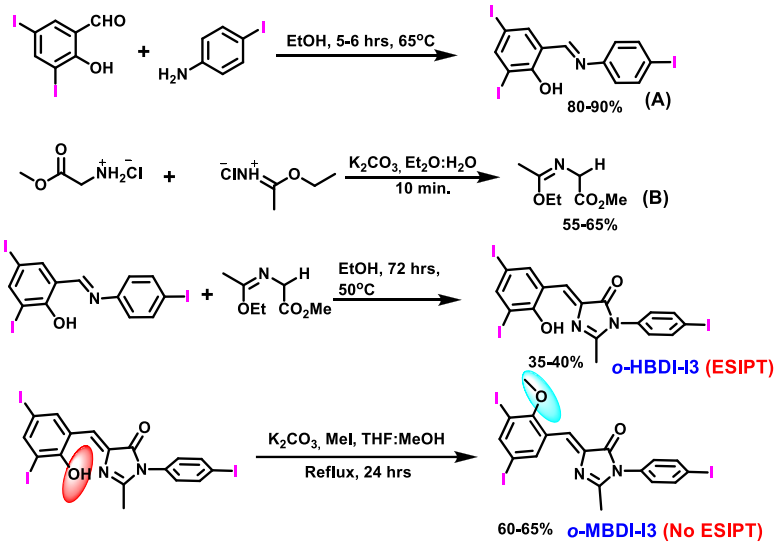

Scheme S1: Synthesis of *gfp* chromophore analogues (*o*-HBDI-I3 and *o*-MBDI-I3).

diiodobenzylidene)-1-(4-iodophenyl)-2-methyl-1H-imidazol-5(4H)-one (*o*-HBDI-I3) and (Z)-4-(3,5-diiodo-2-methoxybenzylidene)-1-(4-iodophenyl)-2-methyl-1H-imidazol-5(4H)-one (*o*-MBDI-I3) were synthesized in the following steps.

2b. Synthesis of ((E)-2,4-diiodo-6-((4-iodophenylimino)methyl)phenol) (A): 2-hydroxy-3,5-diiodobenzaldehyde (3 g, 8.02 mmol) and 4-idoaniline (1.93 g, 8.82 mmol) were mixed together and stirred in ethanol (50 mL) at room temperature for 6 hrs. A red colour precipitate was formed which was filtered off and dried under vacuum at 50 °C for 3 hrs. Yield: 95%. IR (KBr) ν_{max}/cm^{-1}: 3347 (d), 1605 (s), 1278 (m), 1152 (s), 521 (m);^{1}H-NMR (400 MHz, $CDCl_3$) δ: 8.42 (s, 1H), 8.10 (d, J = 1.6 Hz, 1H), 7.75 (d, J = 8.7 Hz, 2H), 7.66 (d, J = 2.0 Hz, 1H), 7.02 (d, J = 8.7 Hz, 2H); ^{13}C NMR ($CDCl_3$, 150 MHz): 80.1, 87.3, 92.7, 120.4, 123.1, 138.7, 140.5, 146.3, 149.3, 160.1, 160.1. ESI-MS+ m/z Calcd. for $C_{13}H_9I_3NO$: 575.7818 $[M+H]^+$, found 575.7813.

2c. Synthesis of methyl-2-(1-ethoxyethylideneamino)acetate (B): Synthesis of methyl-2-(1-ethoxyethylideneamino)acetate was carried out according the reported procedure.[6] In brief, ethylacetimidate hydrochloride (5 g, 40.46 mmol), glycine methyl ester (5.08 g, 40.46 mmol), and potassium carbonate (5.60 g, 40.46 mmol) were taken in 100 ml diethyl ether. The reaction mixture was stirred for 2-4 minutes to make the dispersion. Water (35 ml) was added and further the reaction mixture was stirred for 5 minutes. A clear solution was formed in which the desired product was solubilized in the organic layer (diethyl ether). The organic layer was collected separately. Same procedure was repeated thrice. The organic layer was dried over anhydrous sodium sulphate and solvent was evaporated. A light yellow liquid of methyl-2-(1-ethoxyethylideneamino)acetate was obtained and used for the next step as such. This compound was also characterized by ^{1}H, ^{13}C-NMR, and Mass spectrometry. ^{1}H NMR (400 MHz, $CDCl_3$) δ:1.25 (t, 3H, J = 7.2 Hz); 1.87 (s, 3H); 3.72 (s, 3H), 4.04 (s, 2H); 4.09 (q, 2H, J = 7.2 Hz); ^{13}C NMR (150 MHz, $CDCl_3$) δ : 13.7, 15.2, 51.1, 51.2, 61.0, 165.1, 171.6. ESI-MS+ m/z Calcd. for $C_7H_{14}NO_3$: 160.0974 $[M+H]^+$, found 160.0969.

2d. Synthesis of the *ortho*-hydroxy substituted *gfp* chromophore (*o*-HBDI-I3): (*Z*)-4-(2-hydroxy-3,5-diiodobenzylidene)-1-(4-iodophenyl)-2-methyl-1H-imidazol-5(4H)-one (*o*-HBDI-I3) was synthesized via 2,3-cycloaddition reaction. The compounds ((E)-2,4-diiodo-6-((4-iodophenylimino)methyl)phenol) (1 g, 1.74 mmol) and (methyl-2-(1-ethoxyethylideneamino)acetate) (0.554 g, 3.48 mmol) were mixed in a small amount of

ethanol (15 mL). The reaction mixture was stirred at 50 °C for 48 hrs. A deep red colour of the reaction mixture indicates the formation of *o*-HBDI-I3. The solvent was evaporated and product was dried under vacuum. The crude product was purified by column chromatography. Column purified product was further kept for crystallization in DCM : Methanol (1:3) to get single crystal for X-ray diffraction. The yield of column purified product is 45%. R_f: 0.5 (35% ethyl acetate: hexane). IR (KBr) ν_{max}/cm^{-1} = 3425, 3048, 2929, 2850, 1721, 1637, 1572, 1505, 1437, 1172, 1104, 990, 870, 680, 515. ^{1}H NMR ($CDCl_3$, 600 MHz): δ 2.32 (s, 3H, -CH_3), 7.01 (d, J= 8.4, 2ArH), 7.04 (s, 1H, =CH), 7.59 (s, 1H, -ArH), 7.87 (d, J= 9.0, 2ArH), 8.11 (s, 1H, -ArH).^{13}C NMR ($CDCl_3$, 150 MHz): 29.5, 80.5, 90.2, 95.1, 121.4, 128.7, 128.9, 132.0, 132.9, 139.1, 144.5, 150.4, 157.0, 157.8, 166.2. ESI-MS+ m/z Calcd. for $C_{17}H_{12}I_3N_2O_2$: 656.8027 $[M+H]^+$, found 656.8016.

2e. Synthesis of the *ortho*-methoxy substituted *gfp* chromophore (*o*-MBDI-I3): Methoxy protection of the hydroxyl group of *o*-HBDI-I3 resulted in the compound *o*-MBDI-I3. In brief, the compound *o*-HBDI-I3 (0.450 g, 0.686 mmol) and Na_2CO_3 (0.418g, 3.936 mmol) was taken in 50 mL of solvent mixture of THF: MeOH (4:1). Methyl iodide (0.487g, 3.430 mmol) was added drop wise upon stirring the reaction mixture. The reaction mixture was heated to reflux for 24 hrs. A fluorescent yellow solution was obtained. The reaction mixture was cooled to room temperature and poured into water (150 mL). The compound was extracted with DCM (3-5 times) and subsequently washed thrice from brine solution. Solvent was evaporated and crude product was purified similar to *o*-HBDI-I3. The yield of column purified product is 65%. R_f: 0.5 (30% ethyl acetate: hexane). IR (KBr) ν_{max}/cm^{-1} = 2934, 1710, 1640, 1552, 1485, 1452, 1417, 1251, 1021, 930, 863, 809, 640, 521. ^{1}H NMR ($CDCl_3$, 600 MHz): δ 2.29 (s, 3H, -CH_3), 3.82 (s, 3H, -OMe), 6.99 (d, J= 9.0, 2ArH), 7.36 (s, 1H, -ArH), 7.43 (s, 1H, =CH), 7.85 (d, J= 8.4, 2ArH), 8.11 (s, 1H, -ArH). ^{13}C NMR ($CDCl_3$, 150 MHz): 16.5, 62.7, 89.1, 93.0, 94.4, 119.8, 128.9, 130.4, 132.8, 138.9, 139.6, 141.5, 148.3, 159.8, 162.7, 169.0. ESI-MS+ m/z Calcd. for $C_{18}H_{14}I_3N_2O_2$: 670.8184 $[M+H]^+$, found 670.8187.

2f. Synthesis of 1,3,5-triethynylbenzene (TEB): The synthesis and characterization of 1,3,5-triethynylbenzene was followed according to the procedure reported in literature. The yield of column purified product is 65%. R_f: 0.5 (in hexane), IR (KBr) ν_{max}/cm^{-1} = 3275, 3059, 2105, 1789, 1577, 1415, 1261, 932, 887, 674 cm^{-1}. ^{1}H-NMR ($CDCl_3$, 400

MHz): δ = 7.57 (s, 3H), 3.11 (s, 3H) ppm. ^{13}C-NMR ($CDCl_3$, 150 MHz,): δ = 135.5, 122.9, 81.6, 78.7 ppm. ESI-MS+ m/z Calcd. for $C_{12}H_7$: 151.0548 $[M+H]^+$, found 151.0545.

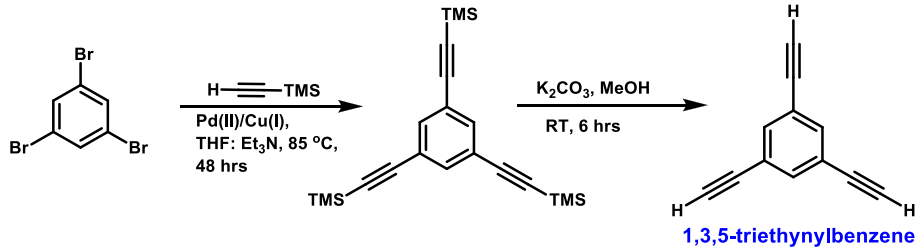

Scheme S2: Synthetic scheme for 1,3,5-triethynylbenzene (TEB).

2g. Synthesis of the *gfp* chromophore analogue containing CMPs (*o*-HBDI-TEB-CMP and *o*-HBDI-TEB-CMP): The synthetic procedure for *o*-HBDI-TEB-CMP and *o*-MBDI-TEB-CMP is similar. Both the CMPs were synthesized by Sonogashira – Hagihara coupling reaction between *o*-HBDI-I3 as well as *o*-MBDI-I3 and 1,3,5-triethynylbenzene (TEB). Chromophore *o*-HBDI-I3 (0.120 g, 0.183 mmol), 1,3,5-triethynylbenzene (0.029 g, 0.183 mmol) and Cu(I) (60 mol%) (0.016 mg, 0.110 mmol) which acts as co-catalyst were taken together in a mix of solvents of dimethyl formamide (DMF) (2 mL) and triethyl amine (1.5 mL). The reaction mixture was purged with N_2 gas for 20 minutes to remove the dissolved oxygen from the solvents. Finally, 30 mol% of Palladium catalyst (Pd(0)) (0.062g, 0.054 m.mol) was added and the reaction mixture was again purged with N_2 for 20 minutes. Reaction mixture was stirred at 135 °C for 24 hrs under inert atmosphere. The reaction mixture was allowed to cool to room temperature and subsequently washed three times with chloroform, THF, methanol and finally with acetone. The resulting CMPs were further purified by Soxhlation in THF for two days. The yield of purified polymer *o*-HBDI-TEB-CMP and *o*-MBDI-TEB-CMP is 80% and 76%, respectively. Further, we have performed EDX and ICP analysis for both the polymers to analyse the presence of residual metal ion (Pd). The EDX analysis shows absence of even trace amount of metal ion in both polymers, *o*-HBDI-TEB-CMP and *o*-MBDI-TEB-CMP (Figure S11). Whereas, ICP analysis shows the presence of 0.87 ppm (0.39 wt%) and 0.97 ppm (0.45%) of Pd in *o*-HBDI-TEB-CMP and *o*-MBDI-TEB-CMP, respectively.

Intra-molecular excited state proton transfer in *o*-HBDI-I3: The proton of –hydroxyl group of *o*-HBDI-I3 undergoes intra-molecular excited state proton transfer to

the imino nitrogen of imidazolinone ring via seven member ring formation.[7] The UV spectrum of *o*-HBDI-I3 in methanol display two bands at 360 nm and 400 nm that are attributed to the enol form (neutral form) and keto form (zwitter ionic species form after ESPT), respectively (Figure 1&S8).[7] The emission spectrum of *o*-HBDI-I3 is collected in methanol upon excitation at 360 nm as well as 400 nm (Figure S8). Two emission peaks are observed at 460 nm and 632 nm which are attributed to the enol form (neutral form) and keto form due to ESPT, respectively. Notably, the emission at 460 nm is found to be very weak and observed mainly in DMSO and MeOH due to hydrogen bonding which perturb the intramolecular ESPT.

On the other hand, *o*-MBDI-I3 compound is not capable for the intra-molecular ESPT due to methoxy substitution. Therefore, the absorption spectrum of o-MBDI-I3 in methanol displays a single absorption maximum at 360 nm (Figure 1). Upon excitation at 360 nm in methanol, the emission maximum is found to be at 470 nm. This further supports that the emission in the red region is subjected to the intra-molecular ESPT.

Lifetime calculations: Lifetime data for monomers (*o*-HBDI-I3 and *o*-MBDI-I3) is fitted using bi-exponential function whereas lifetime data for polymers (*o*-HBDI-TEB-CMP and *o*-MBDI-TEB-CMP) are well suited in tri-exponential function. The average lifetime is calculated using following formula:

$$\textbf{Average life time, } \tau_{avg}(ns) = (\Sigma A_i \tau_i^2 / \Sigma A_i \tau_i)$$

Where, τ_{avg} = average lifetime in nano-seconds,

ΣA_i = sum of percentage of all the components exist in the excited state,

$\Sigma \tau_i$ = sum of excited state lifetime of all the components

Table ST5: PL lifetime details

Sample	A_1(%)	τ_1(ns)	A_2(%)	τ_2 (ns)	A_3(%)	τ_3 (ns)	τ_{avg} (ns)
o-HBDI-I3	99.2	0.11	0.08	1.14	-	-	0.12
o-HBDI-TEB-CMP	87.0	0.58	7.16	7.74	5.84	2.14	4.1
o-MBDI-I3	99.99	0.011	0.01	0.56			0.01
o-MBDI-TEB-CMP	79.47	0.34	18.12	2.21	2.41	9.3	3.4

The detailed percentage of individual components and their excited state lifetime are given above in the table for all the compounds.

Theoretical calculations:

The density functional theoretical (DFT) calculations are performed to optimize molecular geometries of all model systems. The optimizations are performed in Gaussian09 program[8] utilizing B3LYP exchange-correlation functional[9] in conjugation with 6-31G(d) basis set. Implicit solvent effect of methanol is incorporated into the computations by polarisable continuum model (PCM).[10] Grimme's d3 dispersion is also used to consider weak interactions.[11, 12] The harmonic vibrational frequency analysis of the ground-state optimized geometries is performed to confirm the nature of stationary points. All the frequency analyses reveal no imaginary vibrational mode, indicating the optimized geometries as minima on the potential energy surface (PES). The electronic absorption spectra are calculated using time-dependent DFT method at the B3LYP/6-31G(d) level of theory. For this, solvent effect (water) and dispersive interactions are tackled by PCM and Grimme's d3 methods, respectively.

Considering the experimental results, it can be envisaged that the intra-molecular excited-state proton transfer (ESPT) is observed in the *o*-HBDI-I3 whereas the same process does not occur in the *o*-HBDI-TEB-CMP. This observation intrigues us to perform DFT computations. The computations are performed on monomer *o*-HBDI-I3 and also for repeating unit of *o*-HBDI-TEB-CMP (Figure 4 and S22 – S27). In both cases, keto and enol tautomers are considered for geometry optimization in ground state as well as excited state.

Notably, tri-iodo substitutions of *o*-HBDI-I3 are omitted for optimization to reduce the computational cost. The enol tautomer of *o*-HBDI-I3 is found to be stabilized by 5.8 kcal/mole over keto form in the ground electronic state. However the stability is just reversed in the S_1 excited state where keto form is found to be more stable than its enol form by 3.1 kcal/mol. Therefore, the enol form would be solely populated in the ground state and, upon $S_0 \rightarrow S_1$ excitation, the enol form get converted to keto form smoothly (almost barrierless process) via hydrogen transfer in the excited state. Later, the excited keto form bounces back to the S_0 electronic state leading to a much red-shifted emission due to the intra-molecular ESPT phenomenon. The enol form displays lowest energy vertical excitation from HOMO to LUMO at 391 nm and corresponding emission without considering the intra-molecular ESPT is appeared at 469 nm. However, relaxation of excited state keto form illustrates the intra-molecular ESPT and generated emission in the

red region at 602 nm. Thus, theoretical studies clearly indicate that the experimentally obtained red emission of *o*-HBDI-I3 is attributed to the intra-molecular ESPT.

Further, similar calculations are performed for the repeating unit of polymer *o*-HBDI-TEB-CMP. A monomer unit of o-HBDI-I3 connected with three TEB is considered as a model to depict the photophysics of *o*-HBDI-TEB-CMP theoretically. In the ground sate (S_0), similar to the monomer model, enol form of CMP is found to be stabilized over keto form by 2.9 kcal/mol. Whereas in the S_1 excited state, the energy difference for enol and keto form of CMP model is just in reverse order as was predicted for monomer. The enol form of CMP model is found to be stabilized by 3.7 kcal/mol in comparison to keto form. Thus, the excited state hydrogen transfer to forming keto toutomer from enol in CMP model is found to be energetically unfavorable process. This energy difference is expected to prevent the toutomerization from -enol to -keto form in the excited state and, consequently, the intra-molecular ESPT process is not feasible in the CMP model. The TD-DFT computation for –enol model of *o*-HBDI-TEB-CMP displays electronic transition at 388 nm ($S_0 \rightarrow S_1$) from HOMO to the LUMO and corresponding emission appears at 526 nm which is complied with experimentally results. However, the theoretical emission corresponds to deactivation of the excited state of –keto form of *o*-HBDI-TEB-CMP (after intra-molecular ESPT) is found to be at 632 nm which is not observed experimentally. Thus, the experimental results and theoretical predictions support the absence of intra-molecular ESPT in case of *o*-HBDI-TEB-CMP. A closer inspection of the excited state geometries is performed to understand a possible cause of disparity. Interestingly, in the excited state of enol form of monomer, hydroxyl substituted benzene ring and imidazolinone ring is found to be planar with the dihedral angle of 0.2° and this planar geometry play crucial role for an effective intra-molecular ESPT. However, enol form of *o*-HBDI-TEB-CMP shows structural changes in the excited state and a 5.6° twisting of the hydroxyl containing benzene ring from imidazolinone ring is observed. This geometry change and structural rigidity of chromophore in *o*-HBDI-TEB-CMP could be a crucial factor to prevent intra-molecular ESPT process.

Further insight is made by computing the ground and excited state energies for the repeating unit of *o*-MBDI-TEB-CMP, wherein presence of the methoxy group rules out ESPT phenomenon completely. Similar to *o*-HBDI-TEB-CMP, a methoxy substituted model of repeating unit of *o*-MBDI-TEB-CMP has been considered for computational calculation. The lowest energy electronic transition is observed at 366 nm (HOMO→LUMO) and corresponding emission appeared at 418 nm which is close to the

experimental results. Thus, overall, the theoretical predictions are indeed support the experimental results.

Table ST1. Crystal data and structure refinement for *o*-HBDI-I3 and *o*-MBDI

Identification code	***o*-HBDI-I3**	***o*-MBDI-I3**
Empirical formula	$C_{17}H_{11}I_3N_2O_2$	$C_{38}H_{26}I_6N_4O_5$
Formula weight (M)	655.98	1380.03
Crystal system	Monoclinic	Monoclinic
Space group	C2/c	$P2_1/c$
a (Å)	26.971(3)	4.2188(2)
b (Å)	6.4819(7)	32.6154(16)
c (Å)	22.778(2)	15.1566(8)
α (deg)	90.000	90.000
β (deg)	107.072(7)	92.303(3)
γ (deg)	90.000	90.000
V ($Å^3$)	3806.6(7)	2083.83(18)
Z	8	2
T (K)	298 K	298 K
λ (Mo Kα)	0.71073	0.71073
Dc (g/cm^3)	2.289	2.199
μ ($mm^{-1)}$	4.938	4.518
$\theta_{min}/\theta_{max}$	2.78/ 25.82	2.50/ 24.83
total data	62931	53472
unique reflection	3659	3959
R_{int}	0.0435	0.186
R^a	0.0328	0.0680
R^b	0.0910	0.1039
GOF	1.019	1.125
CCDC No	**1865414**	**1865415**

Table ST2. Bond lengths [Å] for *o*-HBDI-I3

I(2)-C(13)	2.097(5)
I(1)-C(1)	2.106(5)
I(3)-C(15)	2.096(5)
O(1)-H(1)	0.8200

Table ST4. Bond lengths [Å] for *o*-MBDI-I3

I(1)-C(1)	2.112(10)
I(2)-C(13)	2.102(11)
I(3)-C(15)	2.107(10)

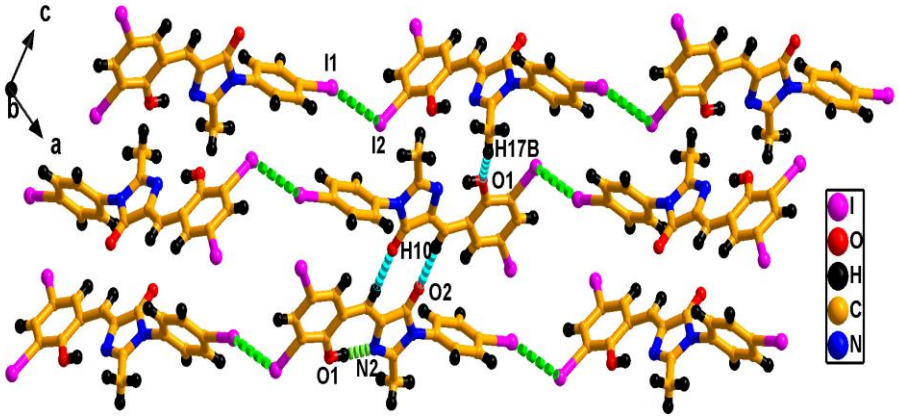

Figure S3: Non-covalent interaction and 2D extended crystal structure of *o*-HBDI-I3.

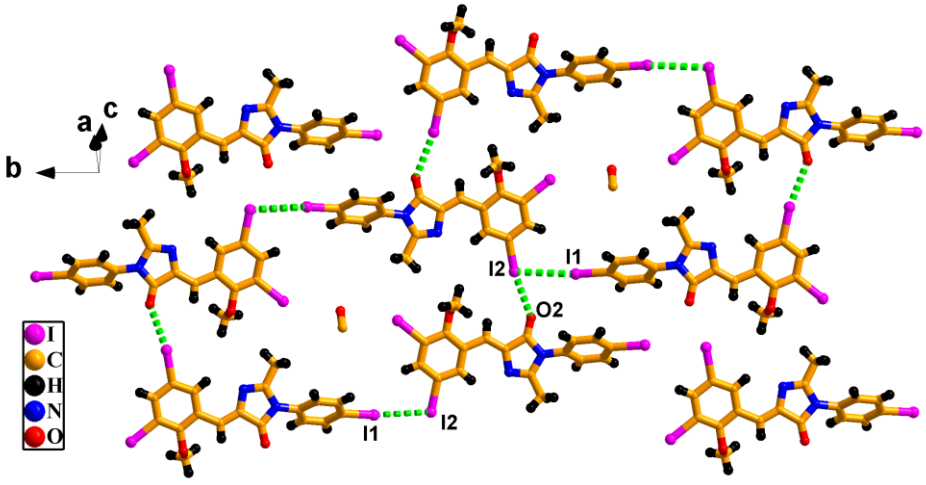

Figure S4: Non-covalent interaction and 2D extended crystal structure of *o*-MBDI-I3.

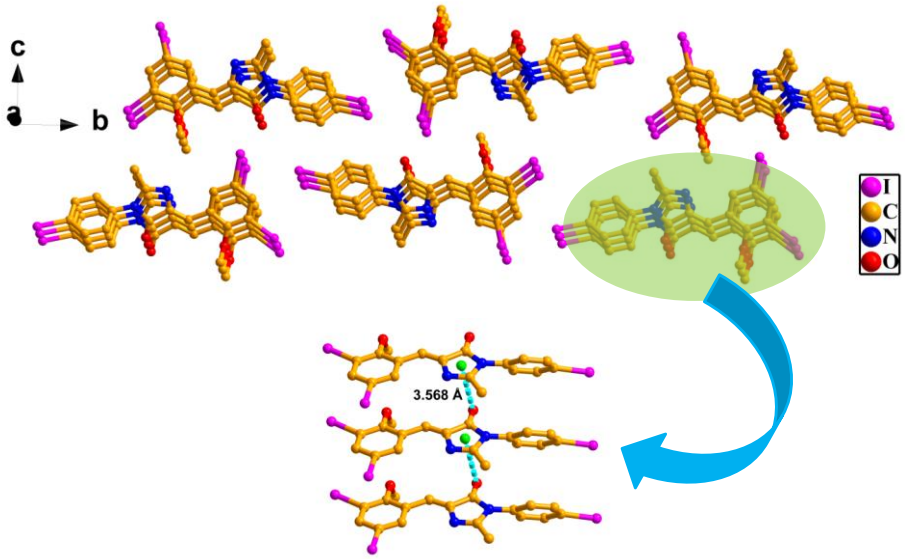

Figure S5: C=O....π interactions in the *o*-MBDI-I3.

^{1}H-NMR and ^{13}C-NMR for *o*-HBDI-I3 monomer:

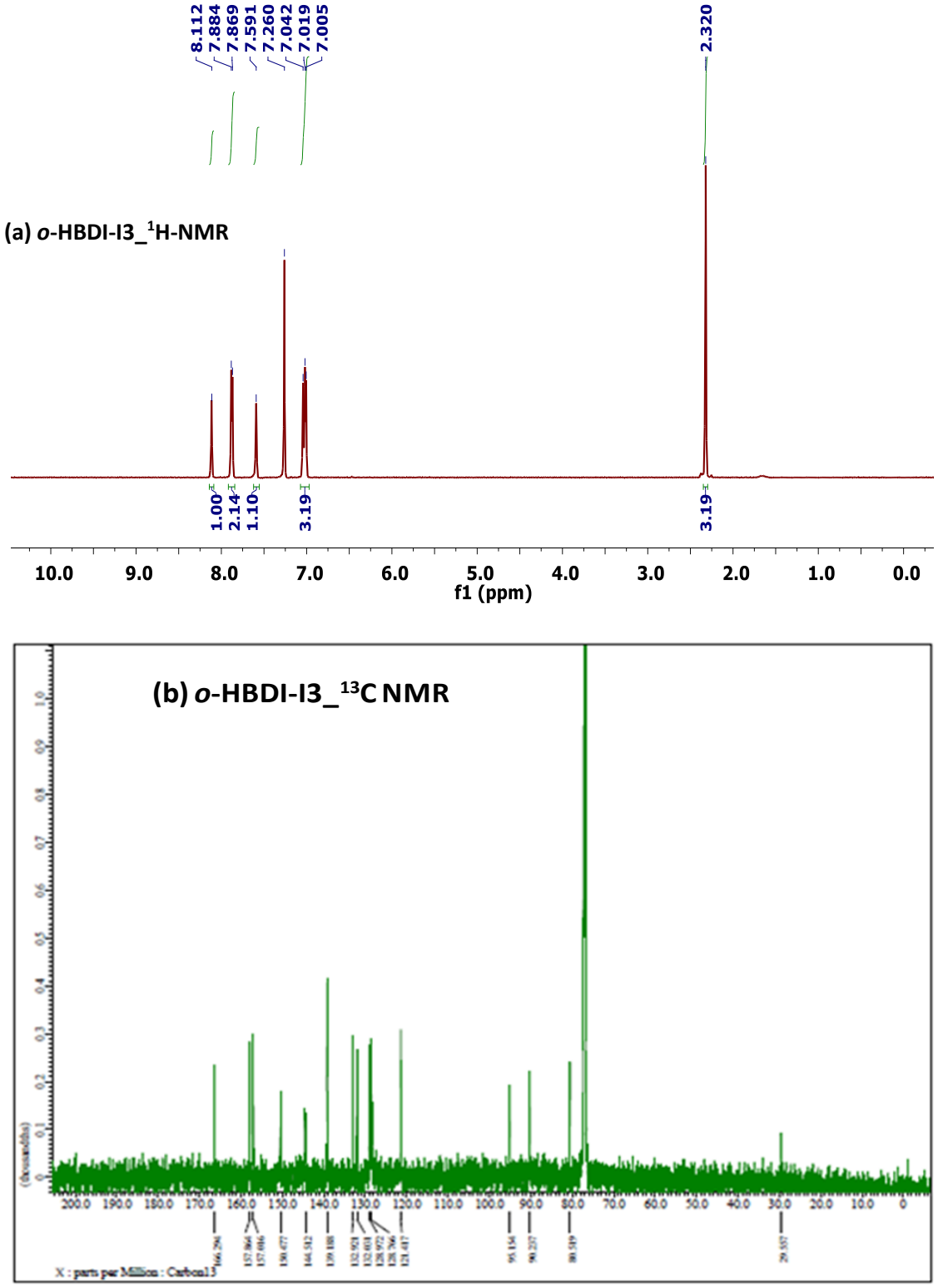

Figure S6: (a) ^{1}H-NMR and (b) ^{13}C-NMR for ***o*-HBDI-I3**, recorded in $CDCl_3$ solvent.

^{1}H-NMR and ^{13}C-NMR for *o*-MBDI-I3 monomer:

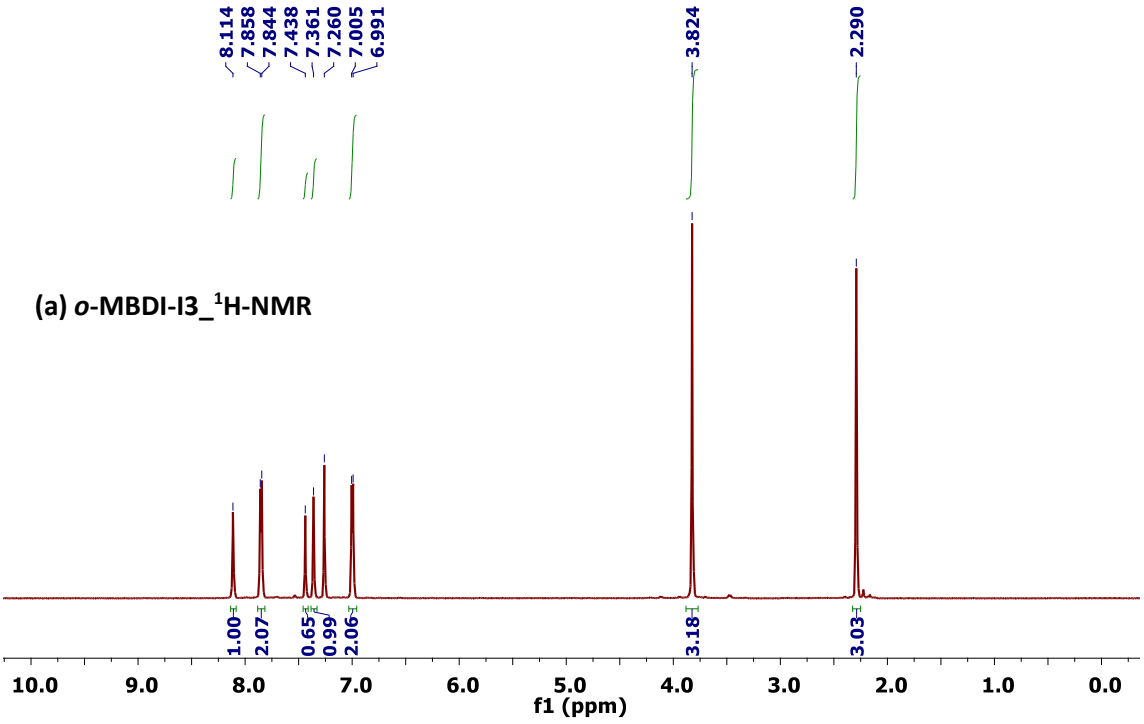

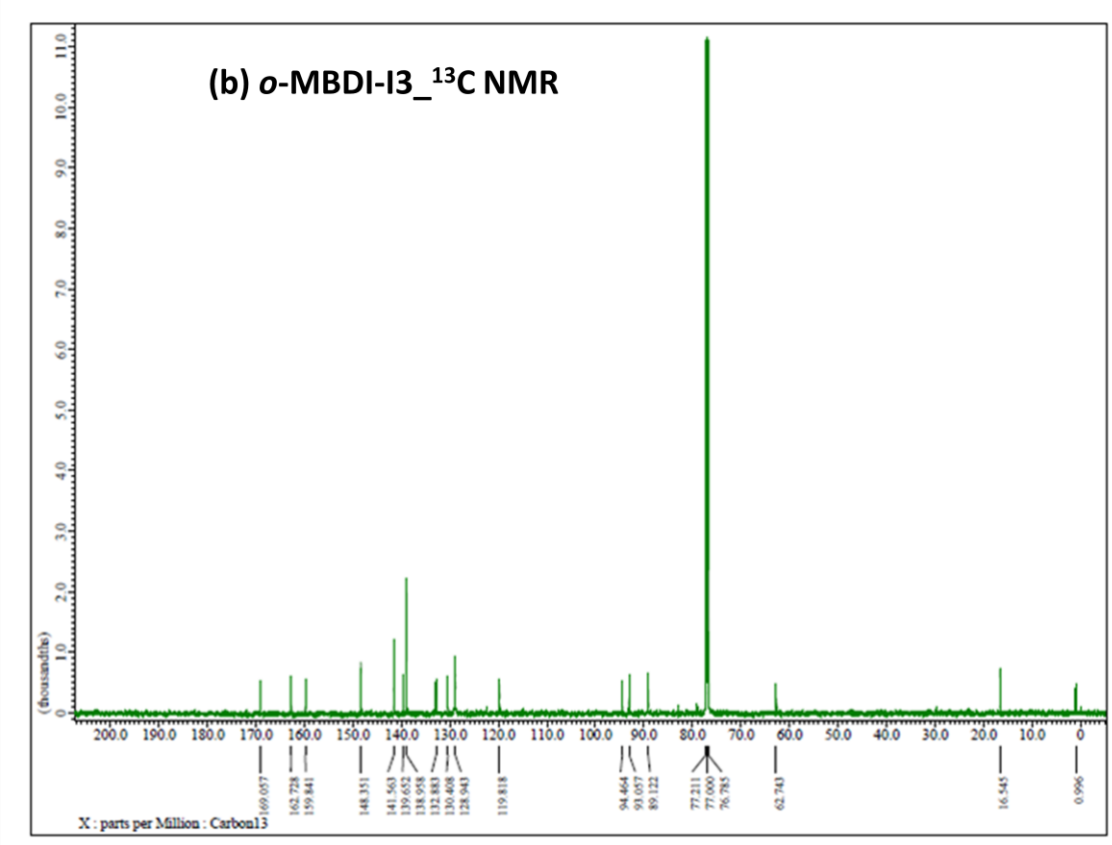

Figure S7: (a) ^{1}H-NMR and (b) ^{13}C-NMR for *o*-MBDI-I3, recorded in $CDCl_3$ solvent.

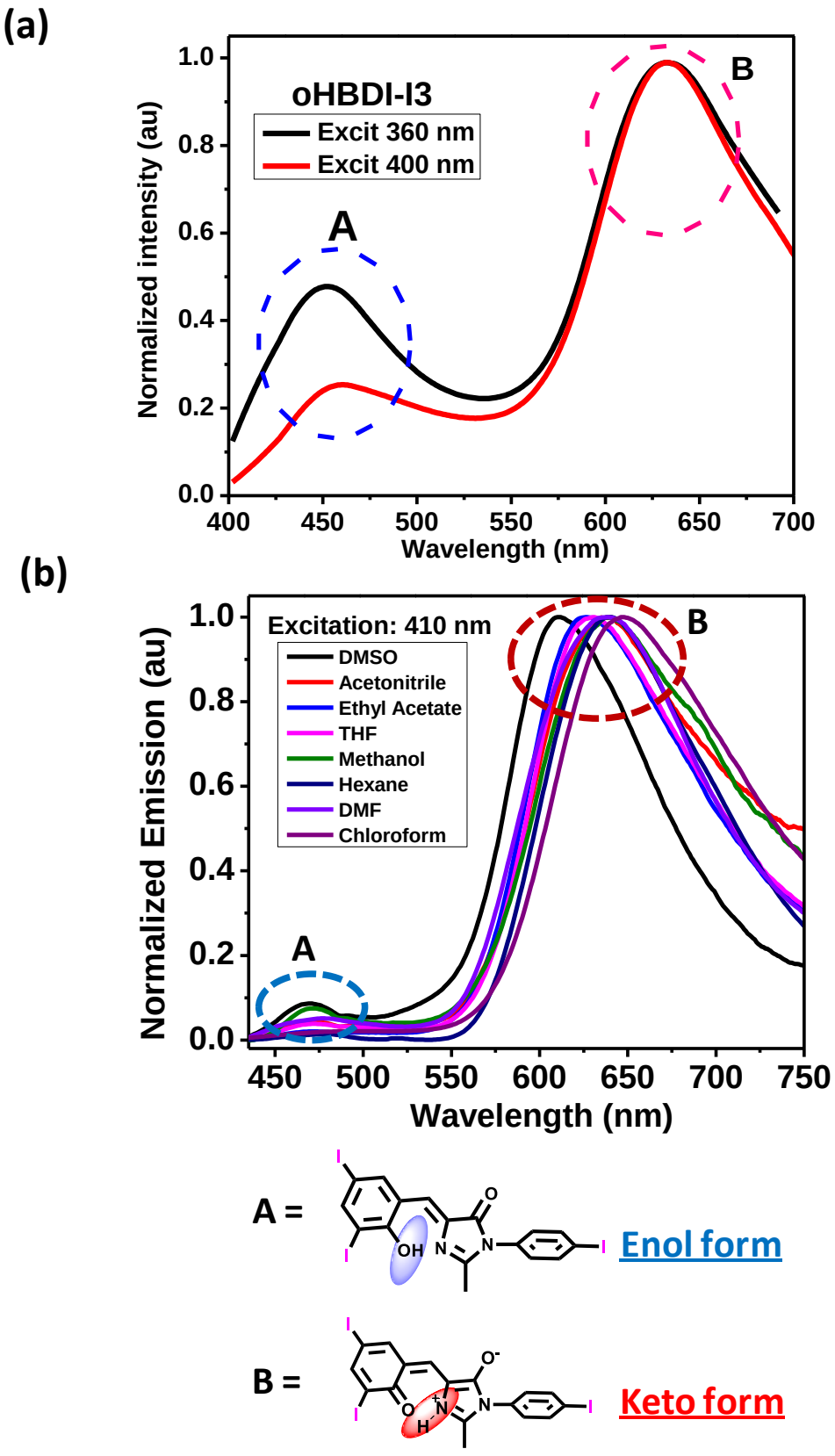

Figure S8: (a) Emission spectra of *o*-HBDI-I3 in methanol at different excitation wavelength (excitation at 360 nm and 400 nm). (b) Solvent dependent emission of *o*-HBDI-I3. All the emission spectra are collected at the concentration of 10^{-5} M.

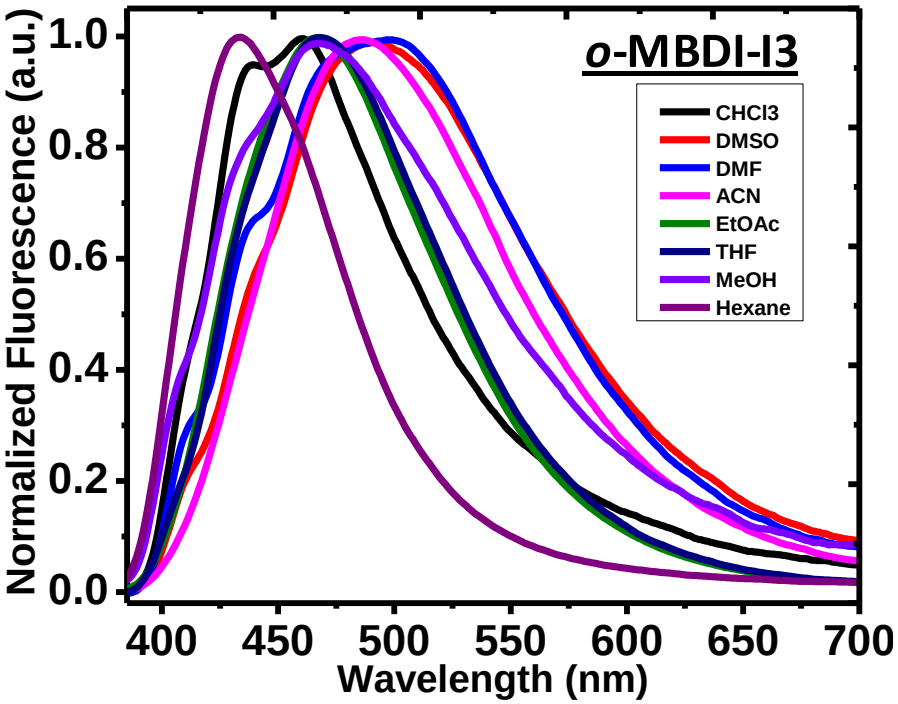

Figure S9: Solvent dependent emission of *o*-MBDI-I3 at the concentration of 10^{-5} M.

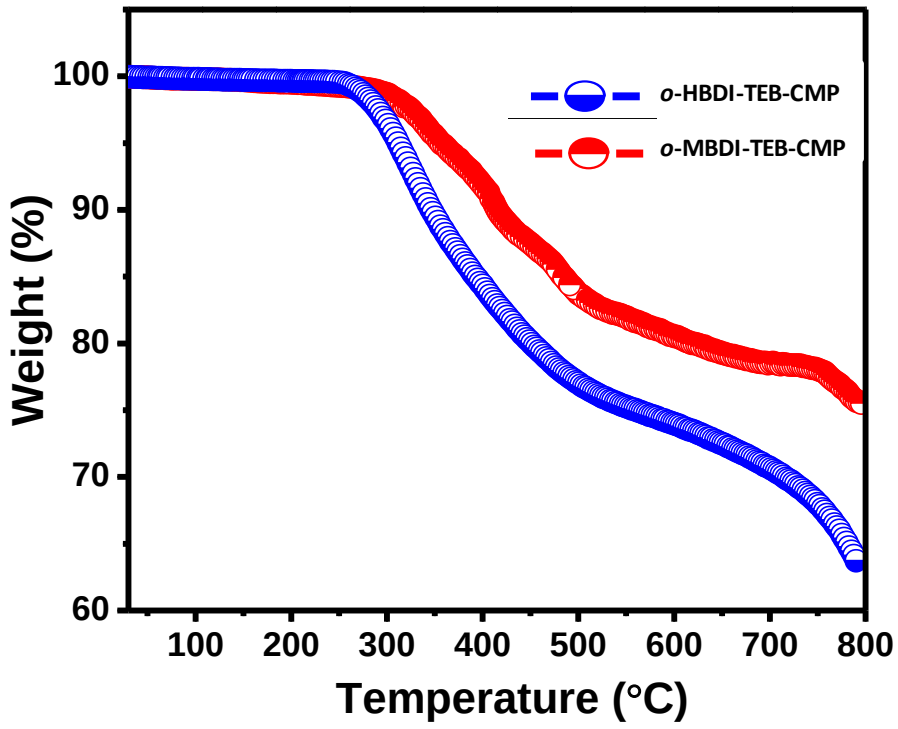

Figure S10: TGA plot for both the polymers; *o*-HBDI-TEB-CMP (blue) and *o*-MBDI-TEB-CMP (red). The TGA is recorded under N_2 atmosphere.

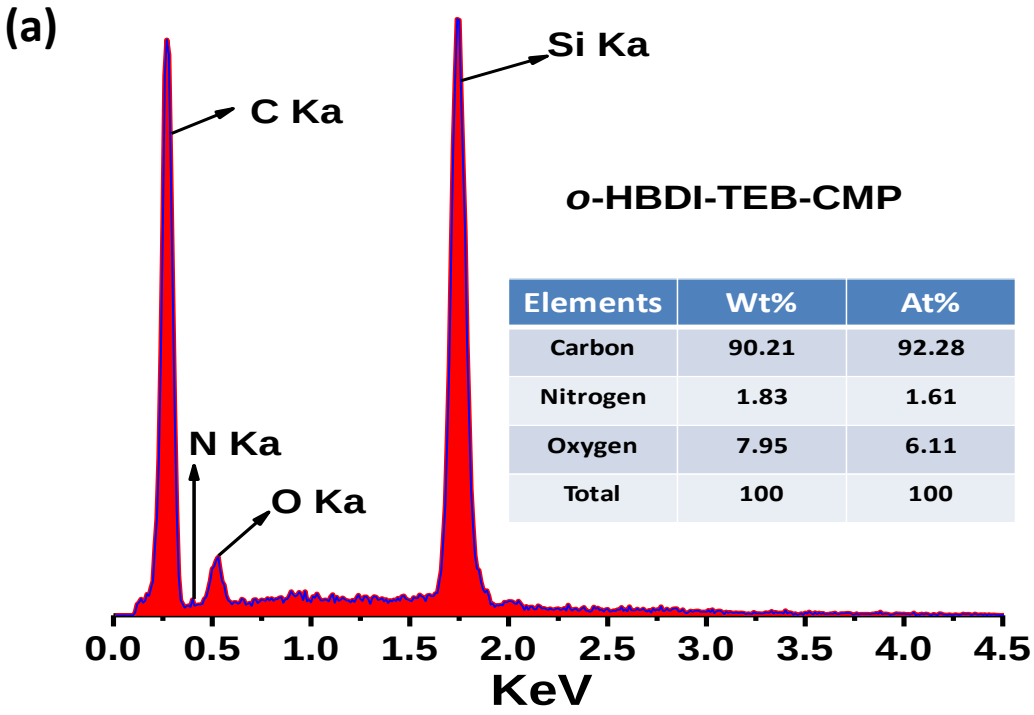

Elements	Wt%	At%
Carbon	90.21	92.28
Nitrogen	1.83	1.61
Oxygen	7.95	6.11
Total	100	100

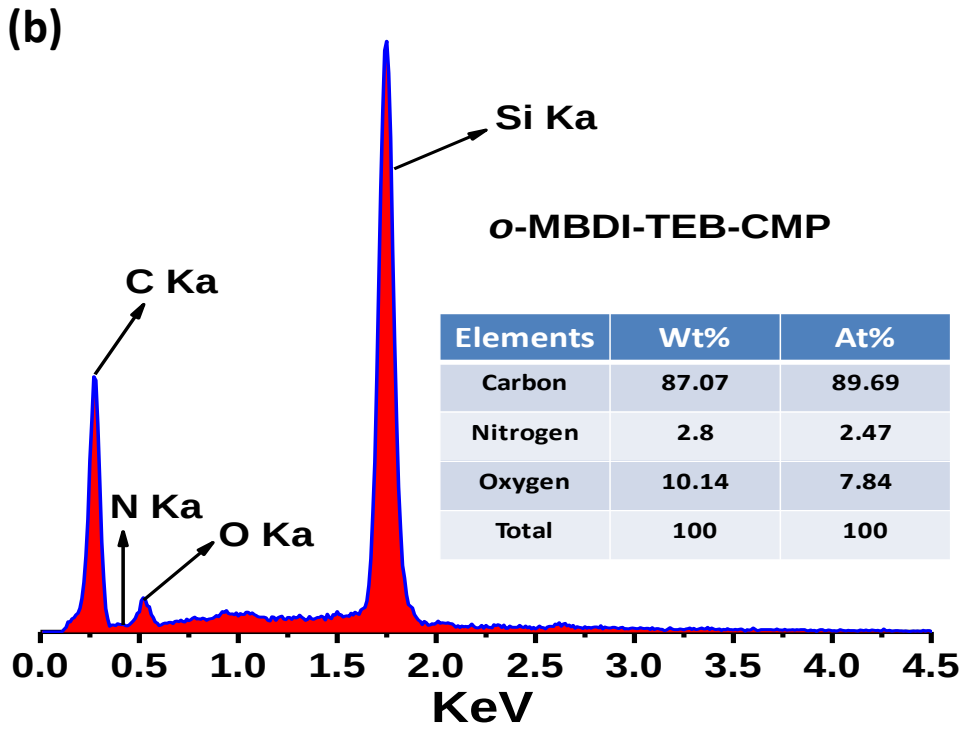

Elements	Wt%	At%
Carbon	87.07	89.69
Nitrogen	2.8	2.47
Oxygen	10.14	7.84
Total	100	100

Figure S11: EDX analysis for (a) *o*-HBDI-TEB-CMP and (b) *o*-MBDI-TEB-CMP

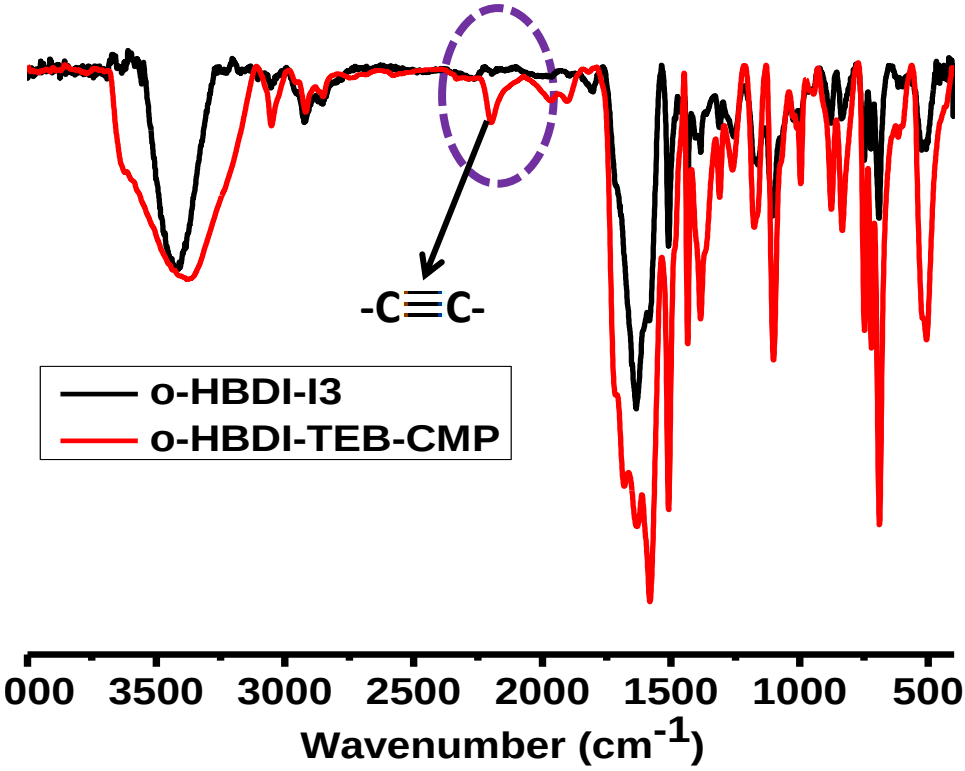

Figure S12: Overlapped IR spectra of *o*-HBDI-I3 and *o*-HBDI-TEB-CMP. Peak in the circled area shows the presence of alkyne bond in *o*-HBDI-TEB-CMP.

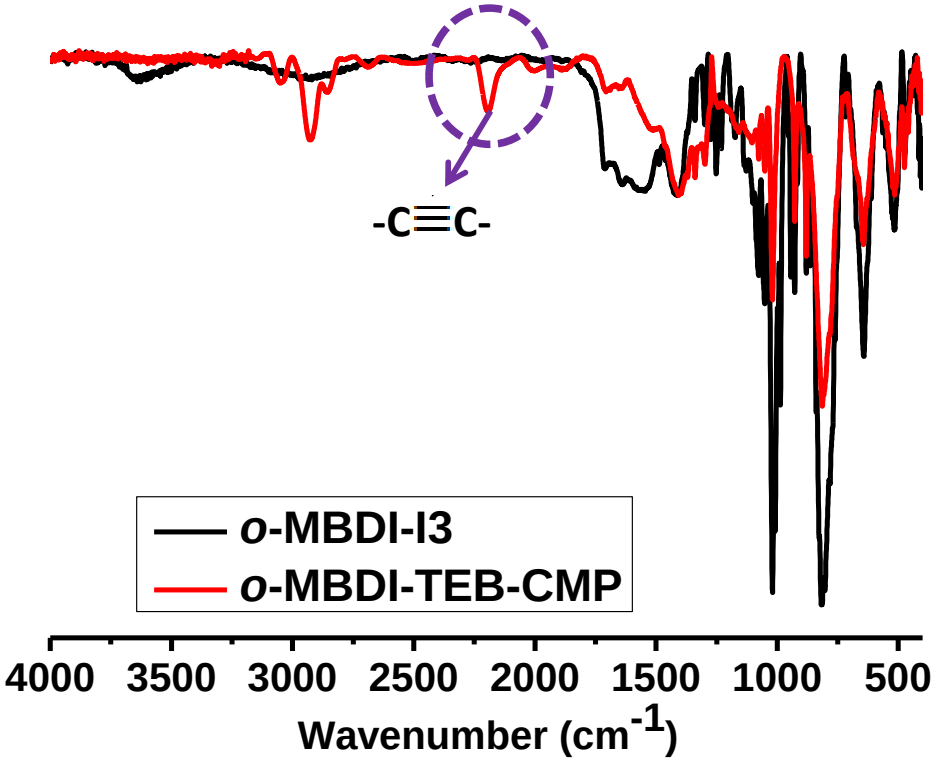

Figure S13: Overlapped IR spectra of *o*-MBDI-I3 and *o*-MBDI-TEB-CMP. Circled area demonstrates the presence of alkyne bond in *o*-HBDI-TEB-CMP.

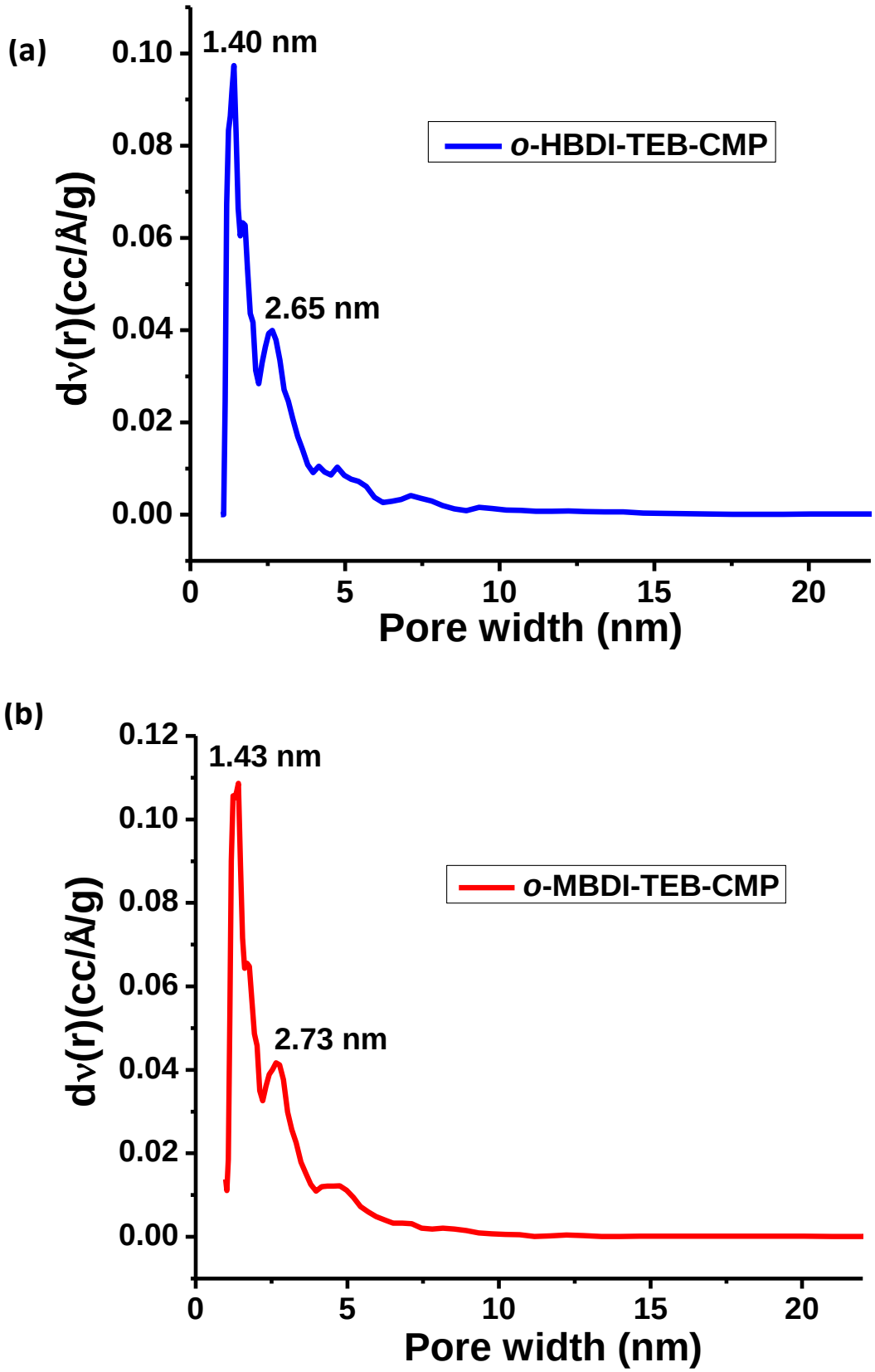

Figure S14: Pore size distribution calculated using NLDFT method for (a) *o*-HBDI-TEB-CMP and (b) *o*-MBDI-TEB-CMP.

UV spectrum:

(a)

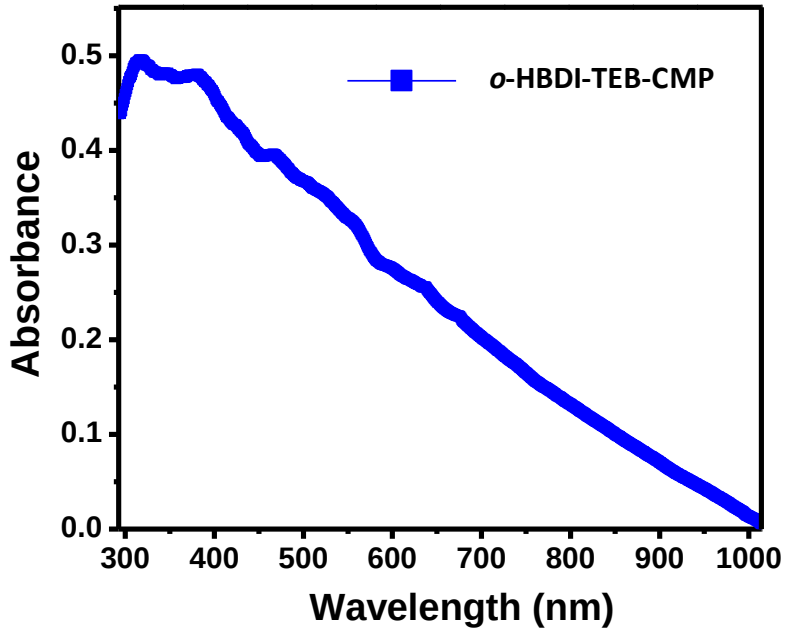

(b)

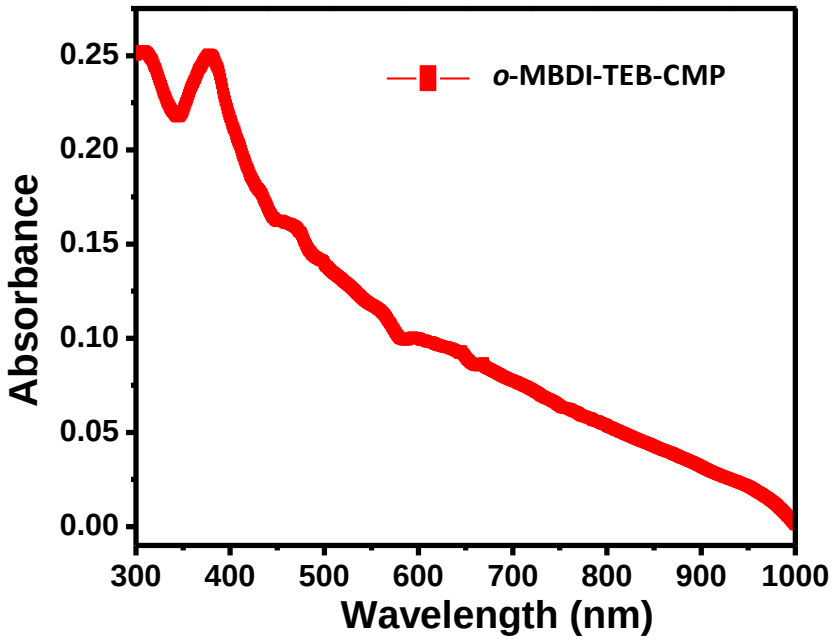

Figure S15: UV-Vis spectrum of (a) *o*-HBDI-TEB-CMP and (b) *o*-MBDI-TEB-CMP, recorded in the dispersed state in MeOH.

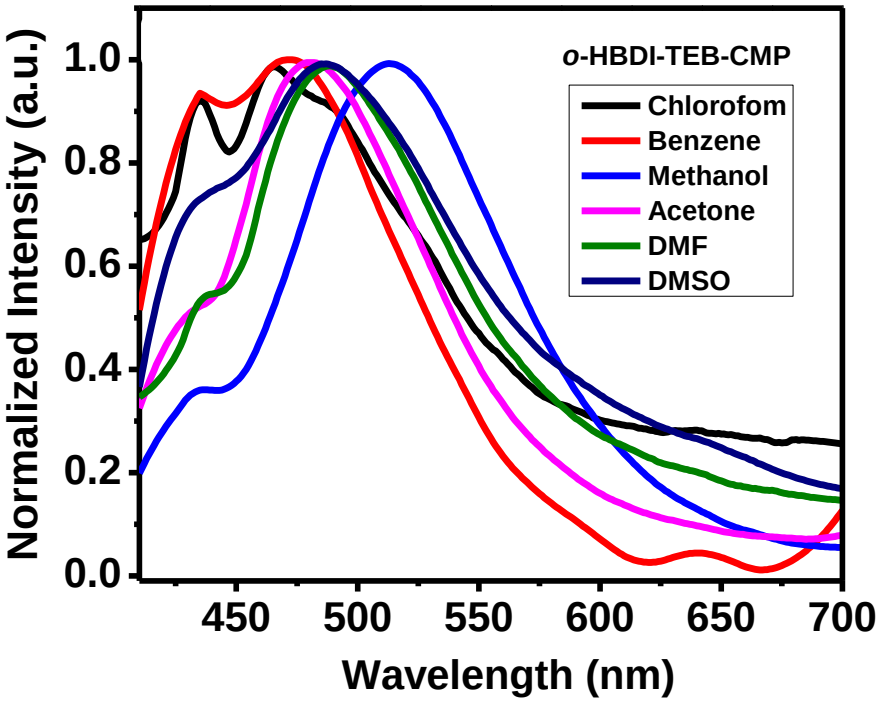

Figure S16: Solvent dependent emissions of *o*-HBDI-TEB-CMP in dispersed state upon excitation at 390 nm.

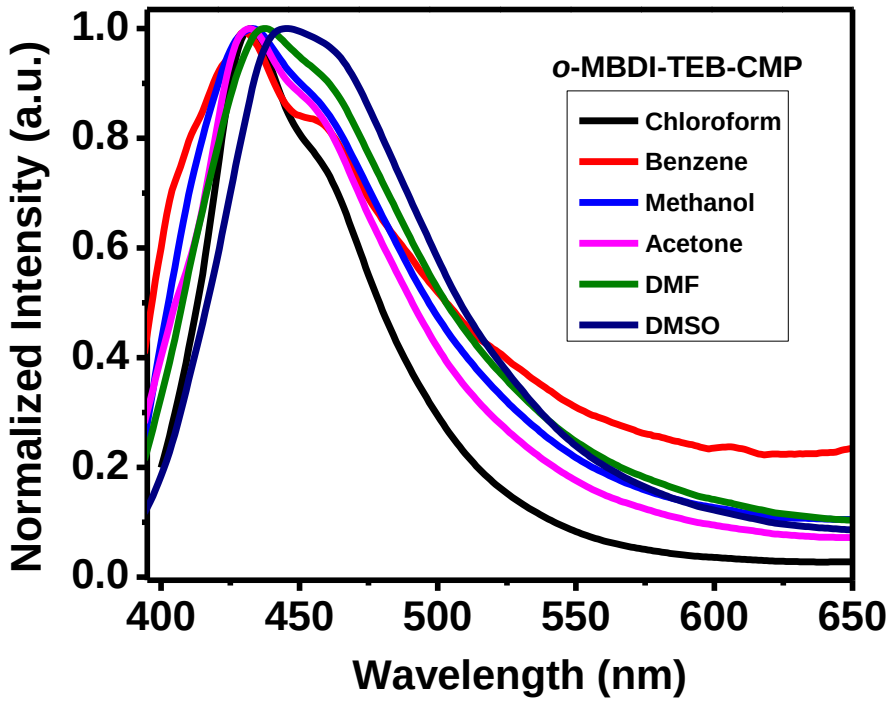

Figure S17: Solvent dependent emissions of *o*-MBDI-TEB-CMP in dispersed state upon excitation at 360 nm.

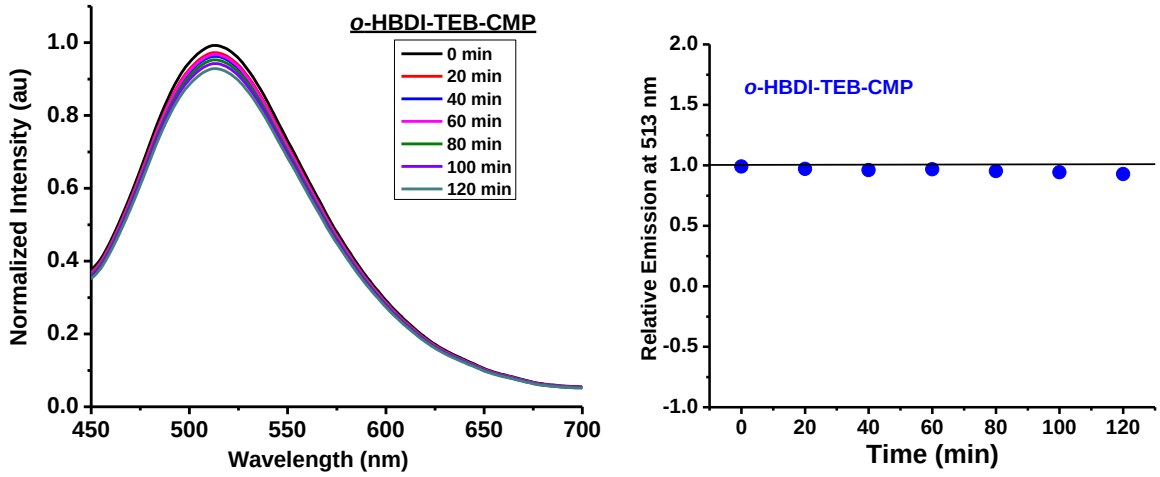

Figure S18: Dispersion stability test for 2 hours for o-HBDI-TEB-CMP in methanol upon excitation at 390 nm. The dispersion is found to be stable with insignificant change in the emission intensity.

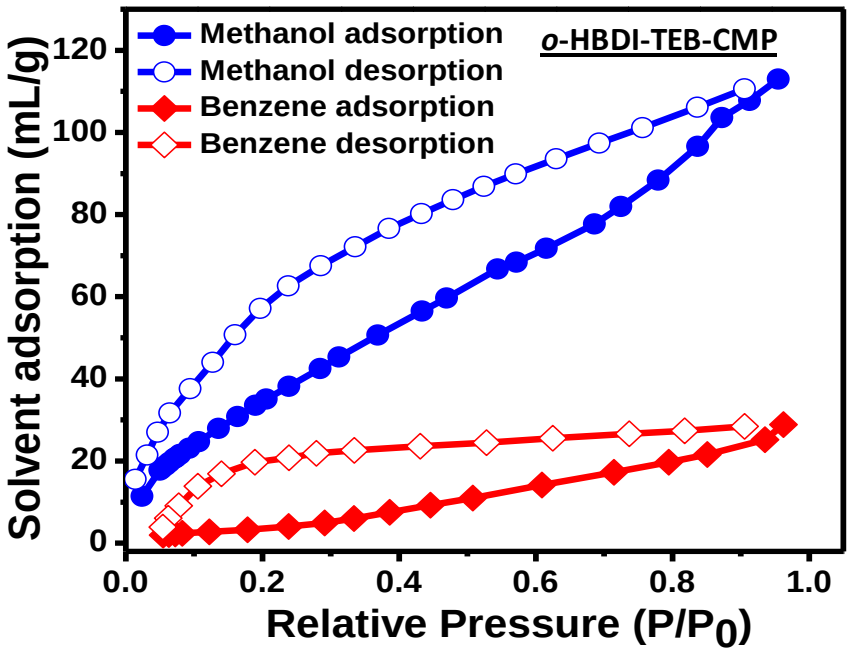

Figure S19: Methanol at 293 K and benzene at 298 K solvent adsorption for *o*-HBDI-TEB-CMP.

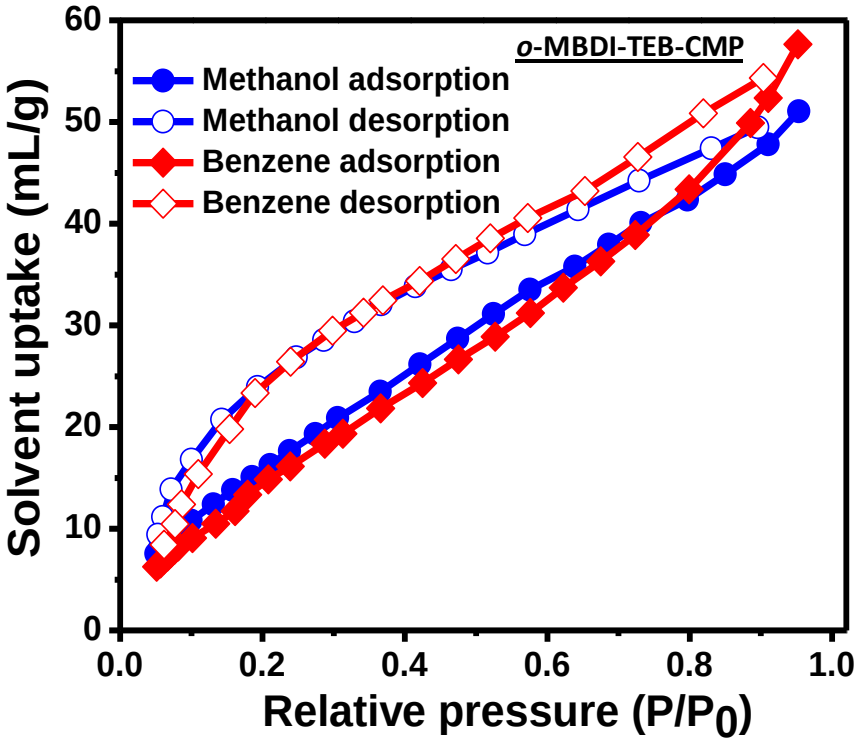

Figure S20: Methanol at 293 K and benzene at 298 K solvent adsorption for *o*-MBDI-TEB-CMP.

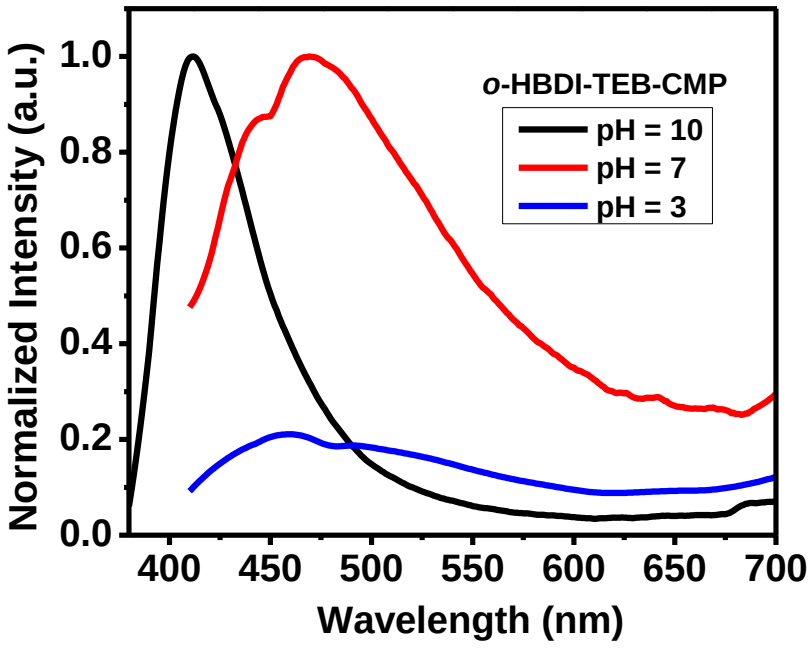

Figure S21: Emission spectra of *o*-HBDI-TEB-CMP at different pH. The neutral pH = 7 was maintained upon addition of 0.2 N HCl in the pH = 10 solution of the *o*-HBDI-TEB-CMP.

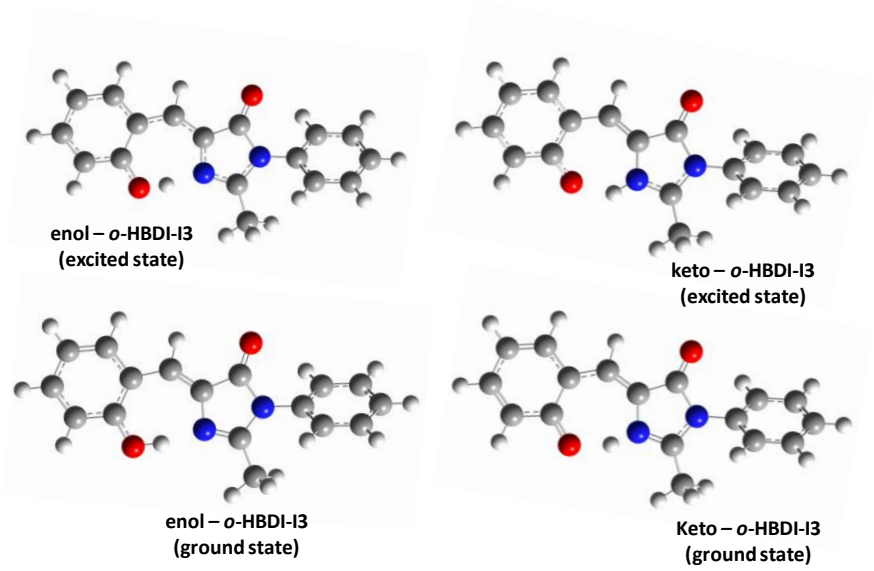

Figure S22: Ground state and excited state geometry optimization for enol and keto form of monomer *o*-HBDI-I3. Iodo-substitutions were not considered for calculation to minimize the computational cost.

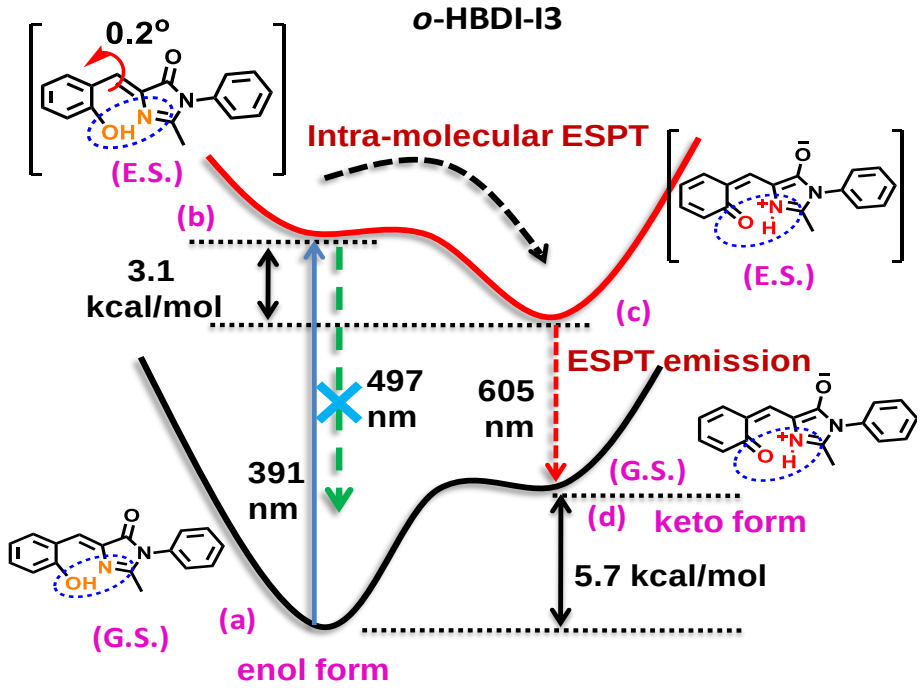

Figure S23: Schematic diagram for theoretically obtained energy differences in methanol for *o*-HBDI-I3. (a) and (b) represent ground state and excited state for enol form, respectively. (c) & (d) represent ground state and excited state for keto form, respectively. Iodo-substitution is not considered in the *o*-HBDI-I3 for calculation to reduce the computational cost. G.S. denotes ground state and E.S. denotes excited state.

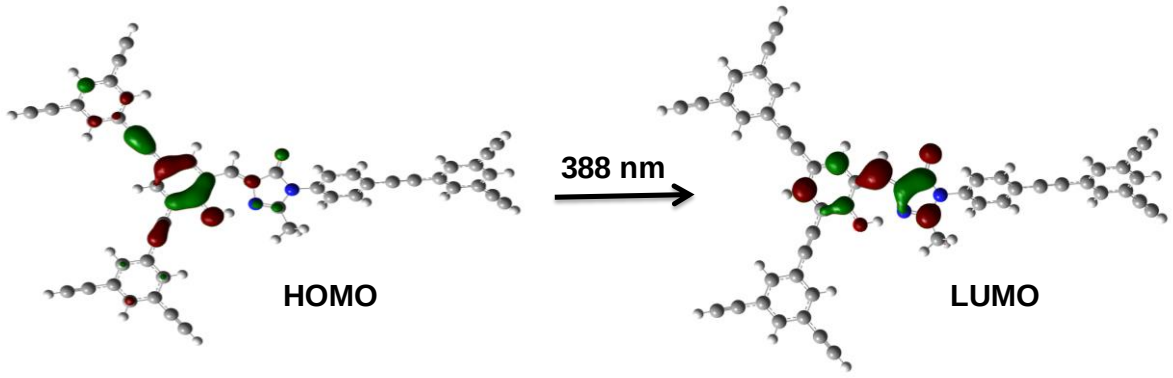

Figure S24: HOMO – LUMO calculation for enol form of polymer *o*-HBDI-TEB-CMP in methanol.

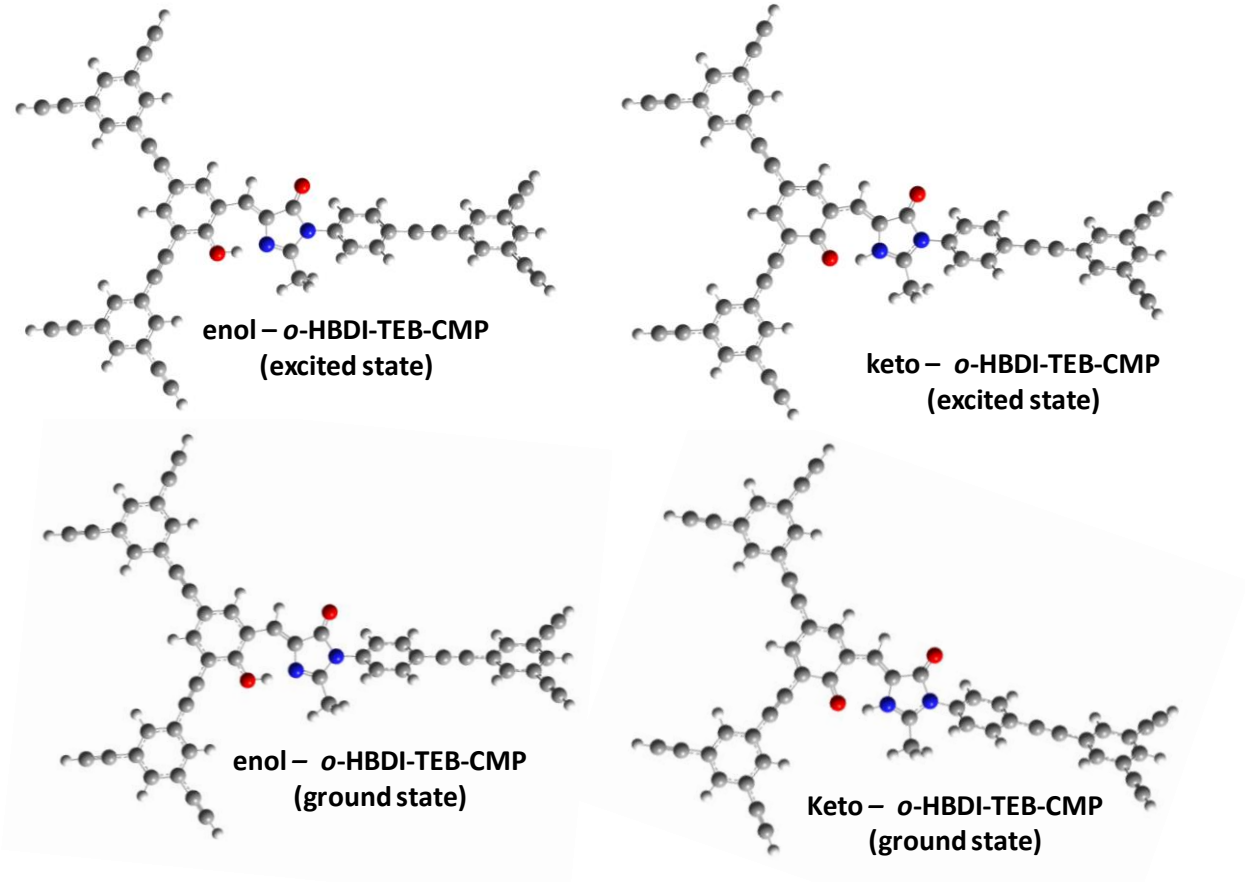

Figure S25: Ground state and excited state geometry optimization for enol and keto form for polymer *o*-HBDI-TEB-CMP in methanol.

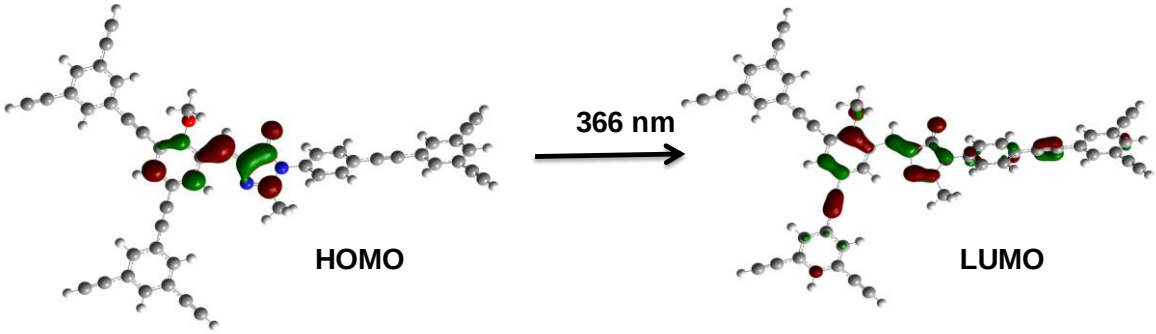

Figure S26: HOMO – LUMO calculation for polymer *o*-MBDI-TEB-CMP in methanol.

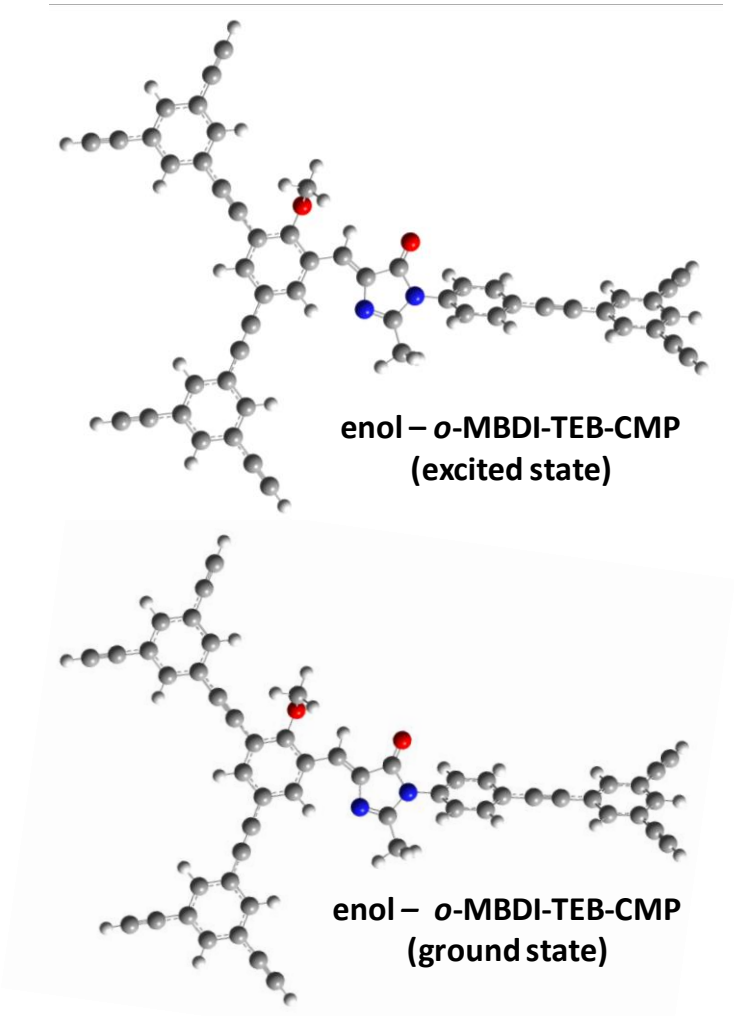

Figure 27: Ground state and excited state geometry optimization for polymer *o*-MBDI-TEB-CMP in methanol.

Reference:

(1) S. V. a. SMART (V 5.628), SAINT (V 6.45a), XPREP, SHELXTL; Bruker AXS Inc. Madison, Wisconsin, USA, **2004**.

(2) Sheldrick, G. M.; SADABS, Empirical Absorption Correction Program. University of Göttingen, Göttingen, **1997**.

(3) Sheldrick, G. M.; SHELXL 97, Program for the Solution of Crystal Structure, University of Göttingen, Germany, **1997**.

(4) Spek, A.; PLATON. *J. Appl. Crystallogr*. **2003**, *36*, 7.

(5) Farrugia, L.; WinGX system, Ver 1.80.05. *J. Appl. Crystallogr*. **1999**, *32*, 837.

(7) Chen, K.-Y.; Cheng, Y.-M.; Lai, C.-H.; Hsu, C.-C.; Ho, M.-L.; Lee, G.-H.; Chou, P.-T.; *J. Am. Chem. Soc*., **2007**, *129*, 4534.

(8) Gaussian 09, Revision D.01, Frisch, M. J.; Trucks, G. W.; Schlegel, H. B.; Scuseria, G. E.; Robb, M. A.; Cheeseman, J. R.; Scalmani, G.; Barone, V.; Mennucci, B.; Petersson, G. A.; Nakatsuji, H.; Caricato, M.; Li, X.; Hratchian, H. P.; Izmaylov, A. F.; Bloino, J.; Zheng, G.; Sonnenberg, J. L.; Hada, M.; Ehara, M.; Toyota, K.; Fukuda, R.; Hasegawa, J.; Ishida, M.; Nakajima, T.; Honda, Y.; Kitao, O.; Nakai, H.; Vreven, T.; Montgomery, J. A. Jr.; Peralta, J. E.; Ogliaro, F.; Bearpark, M.; Heyd, J. J.; Brothers, E.; Kudin, K. N.; Staroverov, V. N.; Kobayashi, R.; Normand, J.; Raghavachari, K.; Rendell, A.; Burant, J. C.; Iyengar, S. S.; Tomasi, J.; Cossi, M.; Rega, N.; Millam, J. M.; Klene, M.; Knox, J. E.; Cross, J. B.; Bakken, V.; Adamo, C.; Jaramillo, J.; Gomperts, R.; Stratmann, R. E.; Yazyev, O.; Austin, A. J.; Cammi, R.; Pomelli, C.; Ochterski, J. W.; Martin, R. L.; Morokuma, K.; Zakrzewski, V. G.; Voth, G. A.; Salvador, P.; Dannenberg, J. J.; Dapprich, S.; Daniels, A. D.; Farkas, Ö.; Foresman, J. B.; Ortiz, J. V.; Cioslowski, J.; Fox, D. J. Gaussian, Inc., Wallingford CT, 2009.

(9) Becke, A.D.; *J. Chem. Phys.*, **1993**, *98*, 5648.

(10) Tomasi, J.; Mennucci, B.; Cammi, R.; *Chem. Rev.*, **2005**, *105*, 2999.

(11) Grimme, S.; Antony, J.; Ehrlich, S.; Krieg, H.; *J. Chem. Phys.*, **2010**, *132*, 154104.

(12) Krukau, A. V.; Vydrov, O. A.; Izmaylov, A. F.; Scuseria, G. E.; *J. Chem. Phys.*, **2006**, *125*, 224106.